Dispersion interactions in proposed covalent superhydride superconductors

Lazar Novakovic, Dean Sayre, Daniel Schacher, Ranga P. Dias, Ashkan Salamat, and Keith V. Lawler

Phys. Rev. B **105**, 024512 — Published 18 January 2022

DOI: 10.1103/PhysRevB.105.024512

Dispersion interactions in proposed covalent superhydride superconductors

Lazar Novakovic,[1] Dean Sayre,[1] Daniel Schacher,[1] Ranga P. Dias,[2,3] Ashkan Salamat,[1,*] and Keith V. Lawler[4,†]

[1] *Department of Physics & Astronomy, University of Nevada Las Vegas, Las Vegas, Nevada 89154, USA*
[2] *Department of Physics & Astronomy, University of Rochester, Rochester, New York 14627, USA*
[3] *Department of Mechanical Engineering, University of Rochester, Rochester, New York 14627, USA*
[4] *Department of Chemistry & Biochemistry, University of Nevada Las Vegas, Las Vegas, Nevada 89154, USA*

(Dated: January 6, 2022)

Recent developments in high temperature superconducting materials under high pressure have made numerical evaluation of the superconducting transition temperature (T_c) of predicted materials critically important as a means to identification. Existing methods of calculating T_c often do not agree with each other or experiment, often due to the large number of complex factors that contribute to this property, among them is the neglect of dispersion interactions in commonly used density functionals. Here, we evaluate the effect of including dispersion interactions on the predicted superconducting properties of two examples of the covalent superhydride class of very high-T_c superconducting materials. In both cases, dispersion is found to have sizeable effects, increasing the electron-phonon coupling as compared to the reference case of elemental niobium. A detailed investigation traces the origin of this effect in a 270 GPa $R3m$ CSH_7 [Cui et al., Phys Rev. B **101**, 134504 (2020)] structure to structural distortions driven by long-range electron-phonon interactions rather than novel bonding networks.

I. INTRODUCTION

Until recently, no stoichiometric metal hydride compound was reported to have a superconducting transition temperature (T_c) beyond 20 K.[1] This led some to initially come to the conclusion that the presence of hydrogen would destroy the superconductivity in such a system due to an uncompensated decrease in the material's electron-phonon coupling (λ) parameter.[2] Despite that, Ashcroft predicted in 2004 that hydrogen dominant alloys could be high-T_c superconductors as they could behave as chemically pre-compressed versions of metallic hydrogen which share its critical properties of a large electron-phonon coupling and a high density of states at the Fermi level related to the hydrogen content.[3–5] Over the last decade, Ashcroft's prediction has been realized as led by the discovery of superconductivity in hydrogen sulfide (H_3S) at 203 K and 155 GPa.[6–8] The explosion of research into superstoichiometric hydride materials have demonstrated the great potential of phonon-mediated superconductors leading up to our own recent report of room temperature superconductivity in a carbonaceous sulfur hydride (C-S-H).[9]

The phonon-mediated superconducting superstoichiometric hydride materials (aka "superhydrides") broadly fall into two classes, metal superhydrides with clathrate-like hydrogen lattices encompassing metal cations,[10–19] and purely covalent superhydrides such as H_3S and C-S-H. The metal superhydrides are often observed as a progression of extended metal hydride phases with increasing hydrogen content as a function of pressure, for instance the synthesis of $YH_{9\pm x}$ following the progression of $Y \rightarrow YH_3 \rightarrow YH_6 \rightarrow YH_{9\pm x}$.[19] On the other hand, the covalent superhydride quantum materials often start their lives as molecular, non-metallic compounds at ambient/low pressure then transform to a pressure induced metallic/superconducting material which still retains some molecular framework. This is most clearly seen with H_3S starting as molecular H_2S or a compound of molecular H_2S and H_2.[6, 20] That molecular structure evolves with pressure into the superconducting extended $Im\overline{3}m$ structure of two interpenetrated perovskite-like SH_3 sublattices which each exhibit a weak 3-dimensional covalency.[6–8, 21–23] Based on the known low pressure molecular solids of CH_4 and H_2,[24] a similar $(H_2S)_{2-x}(CH_4)_xH_2$ molecular solid is believed to be the initial low pressure phase of C-S-H.[9]

Accounting for anharmonic effects has been shown to be important for computing the stability regimes and properties of high pressure superhydrides, especially in resolving the structure of the superconducting phase of H_3S.[25, 26] Likewise, for molecular or layered compounds where van der Waals interactions are present, the treatment of the dispersion interactions is known to be important.[27–34] While present, accounting for dispersion interactions in extended, "hard" materials such as metals and ionic compounds has been shown to not be crucially important for accurate property predictions,[35] and a similar conclusion is anticipated for their superconducting properties. This is especially the case for metal superhydrides which are composed of an extended metallic hydrogen lattice ionically interacting with metal cations. In addition, many classical Lennard-Jones parameterizations have weak interaction energies for hydrogen and transition metals.[36, 37] For example, the nonbonding interaction energies in the Universal Force Field are 0.044 kcal/mol for H, 0.072 kcal/mol for Y, and 0.017 kcal/mol for La, whereas the values for C (0.105 kcal/mol) and S (0.274 kcal/mol) are significantly larger.[36]

* salamat@physics.unlv.edu
† keith.lawler@unlv.edu

Clearly, accounting for dispersion interactions will be important for a consistent description of the covalent superhydrides across all pressures owing to their molecular low pressure phases. However, the importance of dispersion interactions in the high pressure superconducting phases of the covalent superhydrides is unclear. The bonding in H_3S is extended, yet there is no clear interaction between the interpenetrated sublattices.[7, 23] The shortest S—S distance between the sublattices in the first predicted $Im\bar{3}m$ 200 GPa structure (a=2.984 Å)[7] is 2.584 Å, which is slightly longer than a S—S bond and at the intermediate length scale where dispersion interactions should begin to become important. Recent crystal structure prediction simulations on C-S-H have predicted a structure which has a methane (CH_4) molecule intercalated within a single SH_3 sublattice.[38, 39] Accounting for dispersion interactions for such a guest-host structure (ie. with a low dimensional '0-D' sublattice) at lower pressures would be vital for accurate property predictions, and it is likely also the case for the high pressure superconducting phase given the sensitivity of electron-phonon coupling calculations. Herein, we explore the importance of accounting for dispersion interactions in covalent superhydride materials using three benchmark systems: ambient Nb (an elemental, metallic superconductor), the 200 GPa $Im\bar{3}m$ phase of H_3S, and the predicted intercalated H_3S+CH_4 $R3m$ structure for C-S-H at 270 GPa.

II. METHODS

Ab initio plane-wave density functional theory (PW-DFT) [40, 41] simulations for all structural determination and analysis. All structural optimizations were performed as two sequential optimizations followed by a final single-point evaluation resetting the plane-wave basis set between each step to minimize the effect of Pulay stress. The functionals used throughout were the generalized gradient approximation (GGA) of Perdew, Burke, and Ernzerhof (PBE) or the vdW-DF2 van der Waals density functional which accounts for non-local correlation.[42, 43] vdW-DF2 was selected for its documented performance over other non-local vdW density functionals and stock availability in all pertinent modules of Quantum Espresso 6.8. Additional non-local dispersion functionals including vdW-DF [44, 45], rVV10 [46], vdW-DF-cx [47], and vdW-DF3-opt2 [48] were evaluated to confirm the effect of including dispersion interactions. Electron-phonon coupling and superconducting properties were calculated in Quantum Espresso using the linear interpolation and double grid technique.[49–52] Those simulations utilized either the PBE or vdW-DF2 functional as described in the text and the Rappe Rabe Kaxiras Joannopoulos ultrasoft (rrkjus) pseudopotentials formulated for the PBE functional. As ultrasoft pseudopotentials were used, the respective charge density cutoffs (ecutrho) were chosen to be 8–10× the kinetic energy cutoff, which were chosen as discussed below. The self-consistent field convergence threshold was set to 10^{-15} Ry (1.36×10^{-13} eV), and the optimization threshold on forces was 1.2×10^{-6} RyÅ^{-1} (1.63×10^{-5} eVÅ^{-1}). The f_1 and f_2 corrections for the Allen-Dynes equation were calculated using the algebraic simplification of [53].

Evolutionary algorithm crystal structure prediction (CSP) simulations were performed with the USPEX code.[54–56] For each stoichiometry evaluated, the search employed an initial population size of 80 structures, followed by 50 structures for subsequent generations. The optimizations and enthalpy evaluations for the CSP were performed with Vienna *ab initio* simulation package (VASP)[57] version 5.4.4 using the vdW-DF2 functional.[43, 57] For the CSP optimizations, the plane-wave cutoff energy was set to 750 eV, the self-consistent field convergence criterion was 10^{-4} eV, and the forces in the optimizations were converged to 10^{-2} eVÅ^{-1}. The top results from the CSP searches were re-optimized such that all forces were below 10^{-4} eVÅ^{-1}. VASP was also used to generate band decomposed charge densities and band structures. All re-optimizations and analysis simulations used a 1000 eV plane wave cutoff energy, a 10^{-8} eV self-consistent field convergence criterion, an automatically generated Γ-centered k-point grid with 0.3 Å^{-1} spacing, and first order Methfessel-Paxton smearing with a 0.2 eV smearing width.[58] All VASP simulations used the projector augmented wave (PAW) pseudopotentials formulated for GW calculations with PBE.[59, 60] Band and density of state (DOS) plots were made utilizing the SUMO toolkit using paths determined by See-KPATH.[61]

III. RESULTS AND DISCUSSION

Each implementation and modification of electron-phonon calculations in Quantum Espresso have stressed the sensitivity of those calculations to a myriad of values.[51, 52] As this work is intended to compare the results between functionals, and not of the underlying parameters, we will state only that thorough convergence criterion evaluation was performed on all three structures of interest with both functionals and briefly point out a few key results. Significant electron-phonon interactions operate only for electrons near the Fermi surface making good calculations require accurate energies and fine k-point sampling of the Brillouin zone, so optimizations were done several times to check convergence with respect to kinetic energy cutoffs and k-point spacing/grid size. Plane wave cutoffs of 60 Ry, 72 Ry, and 75 Ry were used for the electron-phonon calculations of the Nb, H_3S, and CSH_7 systems, respectively. These were used with corresponding k-point grid samplings of 24×24×24, 25×25×25, 30×30×30, along with q-point grids of 4×4×4, 5×5×5, and 3×3×3. The q-point grids were interpolated to 8× denser grids for T_c analysis. The double-δ smearing parameter has also been highlighted

TABLE I. The calculated superconducting properties of Nb, H_3S at 200 GPa, and CSH_7 at 270 GPa with the PBE and vdW-DF2 functionals. Each structure was optimized in its respective functional prior to evaluating the electron-phonon coupling. The T_cs were calculated using the Allen-Dynes modification of the McMillan equation with μ^*=0.10 (or 0.15).

	Nb		H_3S		CSH_7	
	PBE	vdW-DF2	PBE	vdW-DF2	PBE	vdW-DF2
T_c (K)	13.76 (11.28)	12.61 (10.43)	209.62 (183.06)	202.96 (177.86)	67.43 (43.36)	147.40 (122.78)
λ	1.337	1.410	2.387	2.566	0.732	1.465
$\omega_{\log}$ (K)	123.33	106.04	1060.42	968.51	1675.21	1186.33

as a critical parameter for these simulations.[51, 52] Sufficient smearing width is taken where T_c changes slowest with change in smearing, meaning where T_c peaks as a local maximum, so the appropriate smearing in such a manner for each calculation with a typical value being 0.040 Ry. More details and plots may be found in the Supplemental Materials.[62]

Accounting for dispersion interactions is not expected to have a significant influence on T_c calculations for all superconductors. Thus, a control case is required to test the potential importance of including dispersion interactions for covalent superhydrides beyond the weak description available in semi-local functionals. Niobium is just such a system being the highest temperature elemental superconductor at ambient pressure with a measured T_c of 9.25 K,[63] and previous simulations have established that dispersion corrections are not necessary for an accurate prediction of its T_c from first principles.[51] As intended, the Nb results in Table I show little effect for the inclusion of non-local dispersion effects in the electron-phonon calculations with both functionals slightly overestimating the experimental T_c value, most likely due to the use of the modified Allen-Dynes equation.[64, 65] Using the unmodified McMillan equation which was fit for Nb gives very accurate agreement with respect to experiment for both functionals (Table in Supplemental Materials).[66] The PBE predicted *bcc* lattice for Nb with a=3.315 Å closely agrees with experimental values which are generally reported to be around 3.30 Å.[67] vdW-DF2 expands the lattice constant by 2.4% to 3.379 Å in line with previous simulations,[35] however this expansion has little effect on the predicted T_c. Likewise, the band structure and phonon densities of state as computed in both functionals are also nearly identical (plots in Supplemental Materials). This confirms that much like the structural properties, the superconducting properties of a standard, extended metallic system will not be affected much by accounting for dispersion interactions. It also establishes a baseline expectation of agreement between functionals for such a system to be within ∼1.5%.

Much like Niobium, H_3S is an extended metallic system and thus not expected to have significant dispersion corrections. While the experimentally confirmed highest T_c of 203 K for the proposed $Im\bar{3}m$ phase of H_3S was measured at 155 GPa,[6] the simulations presented here are at 200 GPa to compare with previous theoretical results.[7, 26] The PBE optimized lattice here has a lattice constant of 2.989 Å in good agreement with the results of the previous simulations. In the previous works, the T_cs computed using harmonic phonons and structures with the Allen-Dynes modification of the McMillan equation ranged from 192 K to 204 K for the $Im\bar{3}m$ phase of H_3S. As shown in Table I, the T_c values range from 209.62 to 183.06 K depending on the choice of μ^* in agreement with the initial treatment of Duan *et al.* [7] Their lowest value of 192 K comes from a treatment with μ^*=0.13, and that choice of μ^* shifts our PBE value to 193 K, again in very good agreement with the slight variation stemming from the aforementioned parameterization of the simulation.

The dispersion corrected functional expands the $Im\bar{3}m$ H_3S lattice ($a = 3.020$ Å) relative to PBE while also predicting that it is dynamically unstable at all q-points sampled. Despite the dynamic instability, the electron-phonon coupling of the dispersion corrected simulation is non-negligibly increased ($\lambda = 3.364$) relative to the PBE predicted value. Relaxing this dynamic instability requires the use of a trigonal cell setting within Quantum Espresso, producing the $R3m$ structure of H_3S. The $R3m$ modification contracts the cubic cell's angles to 89.91°, expands the cubic lattice parameter to 3.035 Å, and also contracts the H atoms slightly across the S–H–S bridges towards one of the S atoms. While this contraction appears to form the molecular-like H_3S sub-units characteristic of the $R3m$ phase at lower pressures, the difference of the S–H distances is only 0.26 Å. This makes the non-bonding length significantly shorter than the anticipated hydrogen bonding distance,[68] thus still strongly interacting as reflected in an increased λ relative to the PBE computed value (Table I).

Despite being in the $R3m$ phase, the vdW-DF2 T_c in Table I is similar to that computed with PBE on the $Im\bar{3}m$ structure, with highly overlapping values between the two functionals that could be tuned to experiment through the choice of μ^*. For a single value of μ^* the T_c predicted from the dispersion corrected functional is within ∼3% of that of the semilocal GGA. Inspection of the phonon density of states shows a red-shifting of

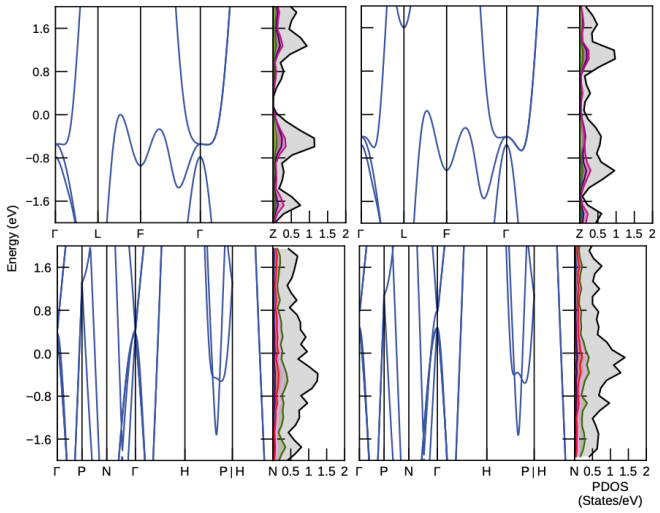

FIG. 1. Calculated band structure and density of states (DOS) near the Fermi level for 270 GPa $R3m$ CSH_7 (top) and 200 GPa $Im\bar{3}m$ H_3S (bottom) with vdW-DF2 (left) and PBE (right). For the DOS of CSH_7, light pink and light blue correspond to carbon s and p states, purple and green to hydrogen s and p states, and dark pink and dark blue to sulfur s and p states, respectively. For the DOS of H_3S, light pink and light blue correspond to hydrogen s and p states, while purple, green and red correspond to sulfur s, p and d states, respectively.

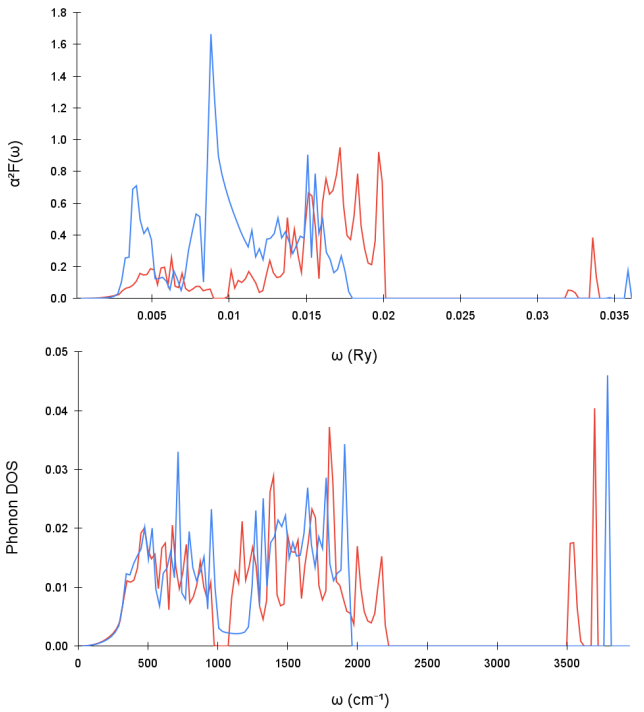

FIG. 2. A comparison of the Eliashberg spectral functions ($\alpha^2F(\omega)$, top) and phonon density of states (PHDOS, bottom) for 270 GPa $R3m$ CSH_7 using PBE (red) and vdW-DF2 (blue).

the dispersion corrected model, and this is somewhat expected from a microscopic Grünesien model point of view as the volume of the vdW-DF2 predicted unit cell is expanded compared to that of the PBE predicted structure. The red-shifting is reflected in the decreased logarithmic average frequency ($\omega_{\log}$), and the differing T_c values reflect a competition between the increased λ but decreased $\omega_{\log}$. More significantly, the Eliashberg spectral function computed with vdW-DF2 is shifted to lower frequency marking the increase in the electron-phonon coupling. Inspection of the electronic structure (Figure 1) of the two representations of the material shows two very similar band structures and densities of state (DOS), but with a more sharply peaked density at the Fermi energy for vdW-DF2. This leads to over 50% more states (1.43 vs .91 states/eV) at the Fermi level in the vdW-DF2 treatment, and a slightly higher total number of states when integrating within an eV of the Fermi level. The increase of states at the Fermi level are the combined H s states and S p states that compose the extended bonding along the individual SH_3 lattices as seen in Figure 1, and can thus be attributed (in part) to the increase in the electron-phonon coupling.

Having established that some difference occurs when dispersion interactions are accounted for in the prediction of superconducting properties, we turn our attention to the key structure of interest, CH_4 intercalated SH_3. This structure was reported as the most stable structure at 150 and 200 GPa by two independent structure searches,[38, 39] albeit in two different space groups. The study of Cui *et al.* [38] explored that further by mapping out the rotational barrier of the CH_4 molecule within the SH_3 lattice of their most favorable $R3m$ structure, finding a very small barrier indicating a weak interaction between the guest CH_4 and the host SH_3 lattice as predicted by a semi-local GGA density functional. Such a weak guest-host interaction from a semi-local approach invokes the possibility of important dispersion interactions in this system. Although several space groups have been suggested for CSH_7 as a function of pressure in the two preceding studies, for this proof of concept study we have chosen to utilize the $R3m$ structure suggested as the most stable phase at 200 GPa for reasons that will be discussed later. For superconducting property analysis, that structure was compressed with both functionals to 270 GPa near where the highest superconducting transition temperature was observed in C-S-H.[9] It should be pointed out that the T_c predicted here by PBE follows along with the trend of the reported PBE determined superconducting dome of $R3m$ CSH_7.[38]

High pressure $R3m$ CSH_7 shows a strong dependence on inclusion of non-local effects in describing superconducting properties. The vdW-DF2 $R3m$ CSH_7 phonon density of states does not shift significantly from the corresponding PBE phonon density of states (Figure 2) and does not indicate any clear conclusion in the phonons, although the phonon dispersion shows vdW-DF2 bands

uniformly shifted to lower frequencies (plot in Supplemental Materials). However, the Eliashberg spectral function in Figure 2 is much more revealing that very different electron-phonon interactions drive the superconductivity in the vdW-DF2 system. A noticeable peak is realized at lower frequencies using the vdW-DF2 functional, which can contribute to the doubling in λ as high densities for lower frequency phonon-mediated interactions correspond to strong electron-phonon coupling. As Coulomb interactions at short ranges become significant, strong electron-phonon coupling should emerge when long-range electron-phonon interactions are dominant. This occurs when the scattering is mediated by phonons of low energy which is reflected in the spectral function as high density in low ω phonon exchange. The result of this combined effect is a doubling of the predicted T_c for any given value of μ^*, unlike in H_3S where only a small variation was seen due to the competing effects of a slightly increased electron-phonon coupling but decreased $\omega_{\log}$. Similar T_c calculations of $R3m$ CSH_7 at lower pressures tended to show dynamic instability and a trend which indicates that 270 GPa is above the peak pressure for this material's superconducting dome (see Supplemental Materials).

TABLE II. A comparison of the calculated superconducting properties of $R3m$ CSH_7 at 270 GPa between several non-local dispersion functionals and PBE ($\mu^* = 0.10$.).

Quantities:	T_c (K)	λ	$\omega_{\log}(K)$
PBE	67.43	0.732	1675.21
vdW-DF3-opt2	73.94	0.7625	1674.76
vdW-DF-cx	74.72	0.766	1674.72
rVV10	81.13	0.797	1668.84
vdW-DF	104.75	0.943	1559.05
vdW-DF2	147.40	1.46	1186.33

Table II shows the superconducting properties (μ^*=0.10) of $R3m$ CSH_7 at 270 GPa calculated with other non-local dispersion functionals. While there is a clear functional dependence to the results produced, the general trend is that accounting for dispersion interactions enhances the computed T_c relative to the PBE value with vdW-DF2 showing the most pronounced effect of all the functionals. For each functional it appears that the increase in the computed λ value is driving the increase in the computed T_c. The increase in λ is clearly more than enough compensation for the lower logarithmic average phonon frequency in each case. A similar evaluation of the rVV10 functional on H_3S also provides results intermediate between PBE and vdW-DF2. Like with vdW-DF2, the $Im\bar{3}m$ structure is dynamically unstable with rVV10 but with smaller magnitude imaginary phonon frequencies. The T_c of the dynamically stable, very slightly distorted $R3m$ H_3S structure is 207.72 K with $\mu^* = 0.10$.

To understand why the inclusion of a dispersion interaction had such an effect on the predicted T_c of CSH_7, we will contrast the differences between the PBE and vdW-DF2 (as it provided the largest response) computed properties of the system. The change in the dispersion included phonon spectrum could be enough to explain the altered Eliashberg spectral function even in the absence of changes in the electronic structure. This is important as the band structure (Figure 1) and electron localization function (ELF, Figure 3) look very similar between both methods. The ELF has been identified as a potential means to quickly estimate the critical temperature of a material,[23] wherein a possible grouping of superconducting materials could be made by determining the highest ELF saturation value that leads to an isosurface which extends across the unit cell in all three dimensions. Here a value of 0.71 is assigned to the PBE ELF of 270 GPa $R3m$ CSH_7, grouping it with the weak covalent hydrogen-hydrogen interaction family of materials known to have high calculated values of T_c. The same saturation value also produces a 3-D bonding network when dispersion interactions are included, and in both cases exceeding this value causes the fully 3-D network to break.

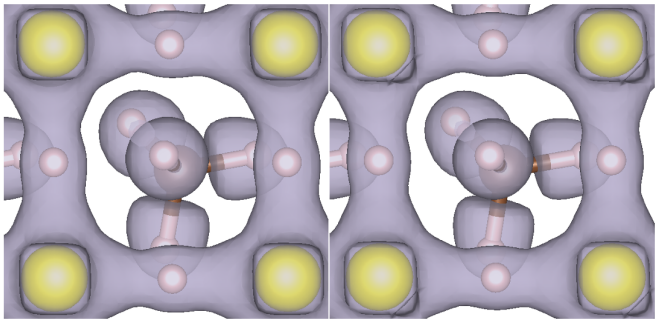

FIG. 3. Calculated electronic localization function isosurfaces for $R3m$ CSH_7 with vdW-DF2 (left) and PBE (right). An isosurface level of 0.71 was chosen to show pipe-like features throughout the shown lattice.

The number of states exactly at the Fermi level differs with 0.510 states/eV for vdW-DF2 and 0.375 states/eV for PBE. However, integrating the entire ~1.5 eV wide metallic band that spans the Fermi level shows a nearly identical number of states, ~184, for both methodologies. The difference is the metallic band according to vdW-DF2 is more sharply peaked at the Fermi level, and the one of PBE is slightly more disperse with much of the density shifted lower in energy. Every channel appears to contribute to this sharp increase in the number of states near the Fermi level for vdW-DF2, not just those of the SH_3 host sublattice. This signals that the CH_4 is not behaving as a non-interacting guest molecule whose states would be semi-valent to the metallic bands describing the bonding in the SH_3 lattice. This increased strength of interaction is also seen in the difference in the standard enthalpy of formation determined by the two functionals, with the vdW-DF2 structure being 0.515 eV

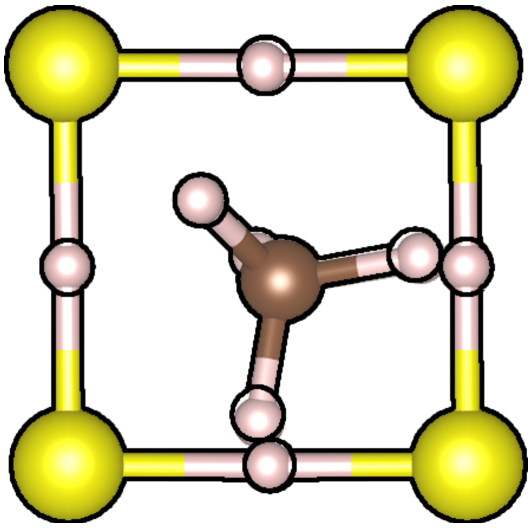

FIG. 4. Structural comparison of the ball-and-stick representation of the PBE optimized $R3m$ CSH_7 structure overlaid with a black outline of the vdW-DF2 optimized structure at 270 GPa.

per formula unit more favorable.[69–71] Not only is the vdW-DF2 representation more energetically favorable, the PBE structure is actually metastable with respect to elemental disproportionation with $\Delta H_f^0 = 0.185$ eV per formula unit. However, in H_3S the standard enthalpy of formation decreases by 0.285 eV per formula unit by from switching to vdW-DF2 from PBE. Thus, it can be interpreted that the formation of the molecular CH_4 unit is more favorable when dispersion is accounted for, and that the dispersion interactions are what are binding the CH_4 to the SH_3 sublattice in the CSH_7 structure.

The stronger interactions between the CH_4 and SH_3 in vdW-DF2 are also manifest in the predicted structure as depicted in Figure 4. The geometry of the $R3m$ structure is best described as a cuboid perovskite-like SH_3 lattice, with three of the CH_4 hydrogen atoms "H2" pointed into one of the faces of the cuboid, while the fourth "H1" points directly at a sulfur atom "S1" of the SH_3 sublattice. In the PBE structure, the S–S nearest neighbor distance in the SH_3 sublattice is 2.852 Å, and those edges are symmetrically bifurcated by H atoms at 1.426 Å. The angles of the SH_3 sublattice are slightly rhombohedrally distorted from a perfect cube by a little under 0.7° with "S1" at the center of the smaller angles. In the vdW-DF2 structure, the rhombohedral distortion of the SH_3 sublattice expands very slightly (still within 0.7°) and the S–S distance elongates to 2.885 Å. However, the H atoms are not symmetrically placed of the center of the S–S distance with the S–H bonds involving "S1" being 0.03 Å longer. In the PBE structure it is the CH_4 unit which is most heavily distorted with a C–H2 distance of 1.024 Å, C–H1 distance of 1.027 Å, the H2–C–H2 angle of 106.8° and H2–C–H1 angle of 112.0°. The vdW-DF2 version of the CH_4 is more regularized with 1.002 Å, C–H1 distance of 1.006 Å, the H2–C–H2 angle of 107.9° and H2–C–H1 angle of 110.0°. Clearly, the absence of non-local interactions is forcing the molecular CH_4 unit to distort heavily to maximize localized interactions with the host SH_3 lattice. In addition to regularizing the CH_4 molecular unit, vdW-DF2 also shifts the C atom slightly closer to the center of the box, however the net result when combined with the expansion of the SH_3 sublattice is an elongation of S1–H1 to 1.713 Å from 1.670 Å. In fact all of the H atoms of the CH_4 unit are a few hundredths of Å further away from their closet neighbors in the vdW-DF2 structure, an effect made favorable by the inclusion of non-local correlations.

The geometric distortions between the PBE and vdW-DF2 structures are so severe that attempting to calculate a T_c in one functional using the other functional's structure produces non-sensical values. For instance, the λ value computed with vdW-DF2 using the PBE structure is in excess of 61.64, and it is 772.50 using PBE with the vdW-DF2 structure. This is most likely due to an excessively large first derivative component present in the evaluation of the phonons, and it highlights the need for very accurate structures when computing T_c values. For H_3S and Nb, the geometric variations between the different structures are minimal enough that a reasonable T_c could be computed (Tables in the Supplemental Materials). For H_3S the cross evaluations of superconducting properties led to a lower T_c, as one would naïvely expect based on previous crystal structure evaluations of phonon-mediation hydrogen-rich high pressure superconductors. Somewhat surprisingly, the cross evaluations of Nb both led to higher T_c values, showing that the effect of non-zero forces can be non-monotonic with regards to the predicted superconducting properties.

The most surprising geometric effect for the vdW-DF2 geometry is the asymmetrization of the SH_3 sublattice despite the regularization of the CH_4 molecular unit. The polarization of the SH_3 sublattice similar to what was seen with H_3S indicates a strong interaction, yet the only noticeable difference between the PBE and vdW-DF2 electronic band structures is more curvature in the highest energy valence band of the PBE calculation near the Γ point as well as lower energies for all k points of the PBE conduction bands (Figure 1 and broader energy range in Supplemental Materials). Figure 5 examines the band decomposed charge densities for the bands near the Fermi level bands to discern why the vdW-DF2 upper most valence band is less dispersive around Γ leading to a more sharply peaked density of states at the Fermi energy. As a note, the labels used in Figure 5 relate to the energy orderings of the bands at the Γ point, with the conduction band maximum (CBM) and CBM+1 being off the scale in Figure 1 and the valence band maximum (VBM) crossing into the conduction bands between Γ and L. The valence band maximum (VBM) and the second highest energy valence band (VBM-1) are degenerate at Γ but show dramatically different interactions. Both VBM-2 and VBM-1 show the extended multi-center bonding along the SH_3 sublattice as is anticipated to be

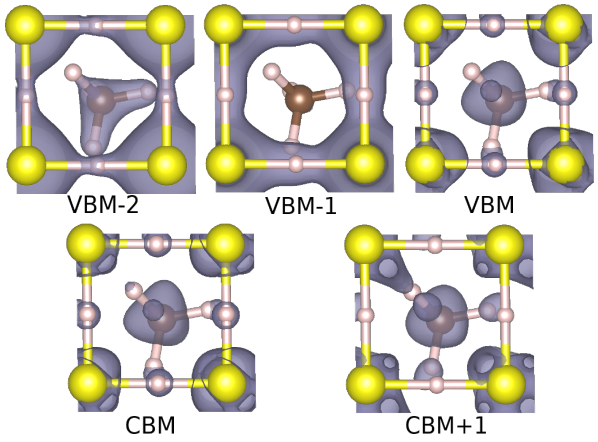

FIG. 5. The vdW-DF2 band decomposed charge density of the three bands in closest proximity to the Fermi energy and the two bands above them in energy of 270 GPa $R3m$ CSH_7. As the system is metallic without distinct valence or conduction bands, the labels relative to the valence band maximum (VBM) and conduction band minimum (CBM) refer to the energy ordering of the bands with respect to the Fermi energy at the Γ point. Each charge density is shown at the 0.018 isosurface level.

near the Fermi level based on the understanding of the bonding in H_3S.[23, 26] VBM-2 has some density on the CH_4 unit, but it is tightly localized and not seen to overlap with that of the SH_3 sublattice unless the isosurface is dropped to 10% of its maximum (0.005). The VBM which has contributions on both the CH_4 unit and the SH_3 sublattice still doesn't show shared charge density between the two units. On the other hand, the PBE versions of these bands look qualitatively similar yet with more polarized densities about the CH_4 units that overlap with the density about the S atoms. The overlapping polarized charge density explain why the CH_4 unit is seen to distort so heavily in the PBE optimized structure.

In the vdW-DF2 simulation it is only what are the conduction bands at Γ that show any direct interaction between the CH_4 and SH_3 sublattices. However, those band indices have no partial occupancy within our model. It should be noted that bands dubbed VBM and CBM cross between Γ and L and again between Γ and F. Inspection of the charge density of those two bands along Γ to L (plot in Supplemental Materials) shows that what is VBM at Γ primarily describes the bonding about SH_3 sublattice and CBM describes the bonding about the CH_4 sublattice. When these bands cross just before L (and F) is when the CH_4 bonding lowers in energy providing that component to the band labelled VBM in Figure 5 which is summed over all $\vec{k}$. At no point along the path in either of those bands is there seen any direct bonding interaction between the two sublattices. Without any evidence of a direct bonding interaction between the two sublattices, the best explanation for the structural distortions seen in the vdW-DF2 SH_3 sublattice is a long-range electron-phonon interaction brought on by trying to increase the dispersion interaction of those H atoms with the CH_4 unit.

Recently, it was proposed that the C-S-H superconducting material is ∼4% carbon doped $Im\bar{3}m$ H_3S.[72] In such a material, the doped C atoms would be anticipated to conform to the bonding network of the S atoms they have replaced, yielding the dual interpenetrated octahedral bonding networks with highly strained C atoms. With the isosurface lowered to 0.012, the VBM more clearly shows a 3-D octahedral bonding network between the CH_4 units, albeit irregular, interpenetrating a 3-D bonding network along the SH_3 sublattice. Such a bonding network on the CH_4 sublattice could easily be interfaced with that of an SH_3 sublattice, raising the possibility that it is methane doping, not carbon replacement, of H_3S that leads to C-S-H.

The reason behind employing the $R3m$ structure for CSH_7 is that complementary crystal structure prediction (CSP) simulations using the vdW-DF2 functional at 270 GPa were performed as part of this work. Only a limited wedge of compositional space was explored, guided by the previous CSP results, including 1 and 2 formula units of $C_xS_yH_z$ stoichiometries where x=1–2 and y=1–2. The choice of z was limited to z=6–9 if x+y=2, and z=9–14 if not. Of the phases explored, the majority of stoichiometries are composed vastly of low-symmetry metals or semi-metals, indicating a preference towards low-dimensionality within a carbonaceous sulfur hydride system with at least a 75% of the atomic constituents being hydrogen. Despite the search space, the most favorable structures belong to the CSH_7 composition. The previously reported Cm CSH_7 was found to be slightly more favorable than the $R3m$ in the initial CSP simulations, but the final high accuracy refinement optimizations for the T_c calculations found the $R3m$ structure to be the most favorable by less than 20 meV per formula unit. In addition to a lower stability, the T_c of the Cm structure was found to be markedly lower than that of the $R3m$ structure at 17.80-14.35 K (for μ^*=0.10–0.15), ruling it out as a potential candidate for C-S-H.

Other than the two aforementioned structures, our confined structure search found variations of low symmetry structures (i.e. molecules in a box and one-dimensional chains) far above the convex line. In particular, it found Pc and $P1$ CSH_7 solutions, both more than 0.9 eV per formula unit above the more favorable CSH_7 structures. For that reason their respective T_cs are not calculated. It's important to note that the $Pmna$ CSH_7 structure found by Cui *et al.* [38] was not evident in our phase space search as were the Cm and $R3m$ motifs. This observation is likely due to either less favorable dispersion interactions or a more highly strained bonding network between the CH_4 sublattice owing to the orientation of the CH_4 units. Thus our work shows that the inclusion of dispersion in systems with expected non-local interactions does not only influence the calculated value of the T_c, but also alters the possible stable and meta-stable structures as

predicted by crystal structure prediction.

IV. CONCLUSIONS

In high pressure condensed matter simulations, the generalized gradient approximation is ubiquitous. This is because as a system becomes more dense, the semi-local treatment is often sufficient to produce an accurate depiction of the physics of the material. However, generalized gradient approximations are known to treat non-local interactions, such as dispersion, poorly which have been shown to be important in modelling low-Z molecular systems even at extreme pressures and temperatures.[73, 74] This proof-of-concept study has shown that accounting for non-local dispersion interactions can be important for predicting the properties of systems that aren't fully molecular but have either a low dimensional sublattice or have non-bonded, weakly interacting sublattices. For both of the potential covalent superhydrides evaluated here, the inclusion of dispersion was found to have the effect of raising the strength of the electron-phonon coupling, as well as the predicted T_c for CSH_7. In fact, the inclusion of dispersion leads the $R3m$ CSH_7 structure to closer agreement with the experimentally measured critical temperature of C-S-H than without. Including dispersion interactions only provides subtle changes to the electronic structure of CSH_7, indicating that it is the long-range electron-phonon interactions known to contribute to strong electron-phonon coupling driving the enhancement seen here. Unfortunately, we remain far off from the experimentally measured T_c of C-S-H, meaning that improved canvassing of the C-S-H phase space and/or methodologies to incorporate quantum ionic fluctuations are needed. Likewise, it has been shown that anharmonicity is also an important effect in determining properties such as the electron-phonon coupling in hydrogen-rich systems like the covalent superhydrides,[25, 75–77] so a combined approach accounting for anharmonicity and non-local effects will likely be required to determine the yet unknown identity of C-S-H through properties such as T_c.

V. ACKNOWLEDGEMENTS

This work supported by the U.S. Department of Energy, Office of Basic Energy Sciences under Award Number DE-SC0020303. Computational resources were provided by the UNLV National Supercomputing Institute.

[1] B. Stritzker and H. Wühl, Superconductivity in metal-hydrogen systems, in *Hydrogen in Metals II: Application-Oriented Properties*, edited by G. Alefeld and J. Völkl (Springer Berlin Heidelberg, Berlin, Heidelberg, 1978) pp. 243–272.
[2] M. Gupta, Solid State Commun. **50**, 439 (1984).
[3] N. W. Ashcroft, Phys. Rev. Lett. **21**, 1748 (1968).
[4] N. W. Ashcroft, Phys. Rev. Lett. **92**, 187002 (2004).
[5] R. P. Dias and I. F. Silvera, Science **355**, 715 (2017).
[6] A. P. Drozdov, M. I. Eremets, I. A. Troyan, V. Ksenofontov, and S. I. Shylin, Nature **525**, 73 (2015).
[7] D. Duan, Y. Liu, F. Tian, D. Li, X. Huang, Z. Zhao, H. Yu, B. Liu, W. Tian, and T. Cui, Sci. Rep. **4**, 6968 (2014).
[8] I. Errea, M. Calandra, C. J. Pickard, J. R. Nelson, R. J. Needs, Y. Li, H. Liu, Y. Zhang, Y. Ma, and F. Mauri, Nature **532**, 81 (2016).
[9] E. Snider, N. Dasenbrock-Gammon, R. McBride, M. Debessai, H. Vindana, K. Vencatasamy, K. V. Lawler, A. Salamat, and R. P. Dias, Nature **586**, 373 (2020).
[10] Y. Xie, Q. Li, A. R. Oganov, and H. Wang, Acta Crystallogr., Sect. C **70**, 104 (2014).
[11] F. Peng, Y. Sun, C. J. Pickard, R. J. Needs, Q. Wu, and Y. Ma, Phys. Rev. Lett. **119**, 107001 (2017).
[12] H. Liu, I. I. Naumov, R. Hoffmann, N. W. Ashcroft, and R. J. Hemley, Proc. Natl. Acad. Sci. U.S.A. **114**, 6990 (2017).
[13] A. R. Oganov, C. J. Pickard, Q. Zhu, and R. J. Needs, Nat. Rev. Mater. **4**, 331 (2019).
[14] E. Zurek and T. Bi, J. Chem. Phys. **150**, 050901 (2019).
[15] J. A. Flores-Livas, L. Boeri, A. Sanna, G. Profeta, R. Arita, and M. Eremets, Phys. Rep. **856**, 1 (2020).
[16] Y. Quan, S. S. Ghosh, and W. E. Pickett, Phys. Rev. B **100**, 184505 (2019).
[17] C. Heil, S. di Cataldo, G. B. Bachelet, and L. Boeri, Phys. Rev. B **99**, 220502(R) (2019).
[18] I. Errea, F. Belli, L. Monacelli, A. Sanna, T. Koretsune, T. Tadano, R. Bianco, M. Calandra, R. Arita, F. Mauri, and J. A. Flores-Livas, Nature **578**, 66 (2020).
[19] E. Snider, N. Dasenbrock-Gammon, R. McBride, X. Wang, N. Meyers, K. V. Lawler, E. Zurek, A. Salamat, and R. P. Dias, Phys. Rev. Lett. **126**, 117003 (2021).
[20] T. A. Strobel, P. Ganesh, M. Somayazulu, P. R. C. Kent, and R. J. Hemley, Phys. Rev. Lett. **107**, 255503 (2011).
[21] Y. Li, J. Hao, H. Liu, Y. Li, and Y. Ma, J. Chem. Phys. **140**, 174712 (2014).
[22] Y. Li, L. Wang, H. Liu, Y. Zhang, J. Hao, C. J. Pickard, J. R. Nelson, R. J. Needs, W. Li, Y. Huang, I. Errea, M. Calandra, F. Mauri, and Y. Ma, Phys. Rev. B **93**, 020103(R) (2016).
[23] F. Belli, J. Contreras-Garcia, and I. Errea, arXiv:2103.07320.
[24] M. S. Somayazulu, L. W. Finger, R. J. Hemley, and H. K. Mao, Science **271**, 1400 (1996).
[25] I. Errea, M. Calandra, and F. Mauri, Phys. Rev. Lett. **111**, 177002 (2013).
[26] I. Errea, M. Calandra, C. J. Pickard, J. Nelson, R. J. Needs, Y. Li, H. Liu, Y. Zhang, Y. Ma, and F. Mauri, Phys. Rev. Lett. **114**, 157004 (2015).
[27] J. Moellmann and S. Grimme, Phys. Chem. Chem. Phys. **12**, 8500 (2010).

[28] D. Tunega, T. Bučko, and A. Zaoui, J. Chem. Phys. **137**, 114105 (2012).
[29] J. Klimeš and A. Michaelides, J. Chem. Phys. **137**, 120901 (2012).
[30] S. Ehrlich, J. Moellmann, and S. Grimme, Acc. Chem. Res. **46**, 916 (2013).
[31] B. Santra, J. Klimeš, A. Tkatchenko, D. Alfè, B. Slater, A. Michaelides, R. Car, and M. Scheffler, J. Chem. Phys. **139**, 154702 (2013).
[32] L. Kronik and A. Tkatchenko, Acc. Chem. Res. **47**, 3208 (2014).
[33] M. J. Gillan, D. Alfè, and A. Michaelides, J. Chem. Phys. **144**, 130901 (2016).
[34] S. A. Tawfik, T. Gould, C. Stampfl, and M. J. Ford, Phys. Rev. Mater. **2**, 034005 (2018).
[35] J. Klimeš, D. R. Bowler, and A. Michaelides, Phys. Rev. B **83**, 195131 (2011).
[36] A. K. Rappe, C. J. Casewit, K. S. Colwell, W. A. Goddard, and W. M. Skiff, J. Am. Chem. Soc. **114**, 10024 (1992).
[37] S. L. Mayo, B. D. Olafson, and W. A. Goddard, J. Phys. Chem. **94**, 8897 (1990).
[38] W. Cui, T. Bi, J. Shi, Y. Li, H. Liu, E. Zurek, and R. J. Hemley, Phys. Rev. B **101**, 134504 (2020).
[39] Y. Sun, Y. Tian, B. Jiang, X. Li, H. Li, T. Iitaka, X. Zhong, and Y. Xie, Phys. Rev. B **101**, 174102 (2020).
[40] P. Hohenberg and W. Kohn, Phys. Rev. **136**, B864 (1964).
[41] W. Kohn and L. J. Sham, Phys. Rev. **140**, A1133 (1965).
[42] J. P. Perdew, K. Burke, and M. Ernzerhof, Phys. Rev. Lett. **77**, 3865 (1996).
[43] K. Lee, E. D. Murray, L. Kong, B. I. Lundqvist, and D. C. Langreth, Phys. Rev. B **82**, 081101(R) (2010).
[44] M. Dion, H. Rydberg, E. Schröder, D. C. Langreth, and B. I. Lundqvist, Phys. Rev. Lett. **92**, 246401 (2004).
[45] T. Thonhauser, S. Zuluaga, C. A. Arter, K. Berland, E. Schröder, and P. Hyldgaard, Phys. Rev. Lett. **115**, 136402 (2015).
[46] R. Sabatini, T. Gorni, and S. de Gironcoli, Phys. Rev. B **87**, 041108(R) (2013).
[47] K. Berland and P. Hyldgaard, Phys. Rev. B **89**, 035412 (2014).
[48] D. Chakraborty, K. Berland, and T. Thonhauser, J. Chem. Theory Comput. **16**, 5893 (2020).
[49] P. Giannozzi, S. Baroni, N. Bonini, M. Calandra, R. Car, C. Cavazzoni, D. Ceresoli, G. L. Chiarotti, M. Cococcioni, I. Dabo, A. D. Corso, S. de Gironcoli, S. Fabris, G. Fratesi, R. Gebauer, U. Gerstmann, C. Gougoussis, A. Kokalj, M. Lazzeri, L. Martin-Samos, N. Marzari, F. Mauri, R. Mazzarello, S. Paolini, A. Pasquarello, L. Paulatto, C. Sbraccia, S. Scandolo, G. Sclauzero, A. P. Seitsonen, A. Smogunov, P. Umari, and R. M. Wentzcovitch, J. Phys.: Cond. Matter **21**, 395502 (2009).
[50] P. Giannozzi, O. Andreussi, T. Brumme, O. Bunau, M. B. Nardelli, M. Calandra, R. Car, C. Cavazzoni, D. Ceresoli, M. Cococcioni, N. Colonna, I. Carnimeo, A. D. Corso, S. de Gironcoli, P. Delugas, R. A. DiStasio, A. Ferretti, A. Floris, G. Fratesi, G. Fugallo, R. Gebauer, U. Gerstmann, F. Giustino, T. Gorni, J. Jia, M. Kawamura, H.-Y. Ko, A. Kokalj, E. Küçükbenli, M. Lazzeri, M. Marsili, N. Marzari, F. Mauri, N. L. Nguyen, H.-V. Nguyen, A. O. de-la-Roza andd L Paulatto, S. Poncé, D. Rocca, R. Sabatini, B. Santra, M. Schlipf, A. P. Seitsonen, A. Smogunov, I. Timrov, T. Thonhauser, P. Umari, N. Vast, X. Wu, and S. Baroni, J. Phys.: Cond. Matter **29**, 465901 (2017).
[51] M. Wierzbowska, S. de Gironcoli, and P. Giannozzi, arXiv:0504077v2.
[52] A. M. Shipley, M. J. Hutcheon, M. S. Johnson, R. J. Needs, and C. J. Pickard, Phys. Rev. B **101**, 224511 (2020).
[53] X. Zheng and J. Zheng, Solid State Commun. **306**, 113769 (2020).
[54] A. R. Oganov and C. W. Glass, J. Chem. Phys. **124**, 244704 (2006).
[55] A. O. Lyakhov, A. R. Oganov, H. T. Stokes, and Q. Zhu, Comp. Phys. Commun. **184**, 1172 (2013).
[56] A. R. Oganov, A. O. Lyakhov, and M. Valle, Acct. Chem. Res. **44**, 227 (2011).
[57] G. Kresse and J. Furthmüller, Phys. Rev. B **54**, 11169 (1996).
[58] M. Methfessel and A. T. Paxton, Phys. Rev. B **40**, 3616 (1989).
[59] P. E. Blöchl, Phys. Rev. B **50**, 17953 (1994).
[60] K. Lejaeghere, G. Bihlmayer, T. Björkman, P. Blaha, S. Blügel, V. Blum, D. Caliste, I. E. Castelli, S. J. Clark, A. Dal Corso, S. de Gironcoli, T. Deutsch, J. K. Dewhurst, I. Di Marco, C. Draxl, M. Dułak, O. Eriksson, J. A. Flores-Livas, K. F. Garrity, L. Genovese, P. Giannozzi, M. Giantomassi, S. Goedecker, X. Gonze, O. Grånäs, E. K. U. Gross, A. Gulans, F. Gygi, D. R. Hamann, P. J. Hasnip, N. A. W. Holzwarth, D. Iuşan, D. B. Jochym, F. Jollet, D. Jones, G. Kresse, K. Koepernik, E. Küçükbenli, Y. O. Kvashnin, I. L. M. Locht, S. Lubeck, M. Marsman, N. Marzari, U. Nitzsche, L. Nordström, T. Ozaki, L. Paulatto, C. J. Pickard, W. Poelmans, M. I. J. Probert, K. Refson, M. Richter, G.-M. Rignanese, S. Saha, M. Scheffler, M. Schlipf, K. Schwarz, S. Sharma, F. Tavazza, P. Thunström, A. Tkatchenko, M. Torrent, D. Vanderbilt, M. J. van Setten, V. Van Speybroeck, J. M. Wills, J. R. Yates, G.-X. Zhang, and S. Cottenier, Science **351**, aad3000 (2016).
[61] A. M. Ganose, A. J. Jackson, and D. O. Scanlon, J. Open Source Software **3**, 717 (2018).
[62] See Supplemental Material at [URL will be inserted by publisher] for additional simulation and convergence details, band dispersion and density of state plots, band decomposed charge density plots, phonon dispersion plots, Eliashberg spectral function plots, and additional tabulated comparison data.
[63] D. K. Finnemore, T. F. Stromberg, and C. A. Swenson, Phys. Rev. **149**, 231 (1966).
[64] P. B. Allen and R. C. Dynes, Phys. Rev. B **12**, 905 (1975).
[65] E. F. Talantsev, Supercond. Sci. Tech. **33**, 094009 (2020).
[66] W. L. McMillan, Phys. Rev. **167**, 331 (1968).
[67] R. Roberge, J. Less Common Met. **40**, 161 (1975).
[68] A. Das, P. K. Mandal, F. J. Lovas, C. Medcraft, N. R. Walker, and E. Arunan, Angew. Chem. Int. Ed. **57**, 15199 (2018).
[69] J. M. McMahon and D. M. Ceperley, Phys. Rev. Lett. **106**, 165302 (2011).
[70] H. Luo, R. G. Greene, and A. L. Ruoff, Phys. Rev. Lett. **71**, 2943 (1993).
[71] N. Bindzus, T. Straasø, N. Wahlberg, J. Becker, L. Bjerg, N. Lock, A.-C. Dippel, and B. B. Iversen, Acta Crystallogr., Sect. A **70**, 39 (2014).
[72] Y. Ge, F. Zhang, R. P. Dias, R. J. Hemley, and Y. Yao, Mater. Today Phys. **15**, 100330 (2020).

[73] M. A. Morales, C. Pierleoni, E. Schwegler, and D. M. Ceperley, Proc. Natl. Acad. Sci. U.S.A. **107**, 12799 (2010).
[74] C. Pierleoni, M. A. Morales, G. Rillo, M. Holzmann, and D. M. Ceperley, Proc. Natl. Acad. Sci. U.S.A. **113**, 4953 (2016).
[75] I. Errea, M. Calandra, and F. Mauri, Phys. Rev. B **89**, 064302 (2014).
[76] R. Bianco, I. Errea, L. Paulatto, M. Calandra, and F. Mauri, Phys. Rev. B **96**, 014111 (2017).
[77] L. Monacelli, I. Errea, M. Calandra, and F. Mauri, Phys. Rev. B **98**, 024106 (2018).